Step-induced double-row pattern of interfacial water on rutile TiO_2(110) at electrochemical conditions

Yan Sun[1], Cheng-Rong Wu[1], Feng Wang[1], Rui-Hao Bi[1], Yong-Bin Zhuang[1], Shuai Liu[1], Ming-Shu Chen[1], Kelvin H.-L. Zhang[1,2,*], Jia-Wei Yan[1,*], Bing-Wei Mao[1], Zhong-Qun Tian[1,2], and Jun Cheng[1,2,*]

[1]State Key Laboratory of Physical Chemistry of Solid Surfaces, iChEM, College of Chemistry and Chemical Engineering, Xiamen University, Xiamen 361005, China
[2]Innovation Laboratory for Sciences and Technologies of Energy Materials of Fujian Province (IKKEM), Xiamen, China
[*]chengjun@xmu.edu.cn; jwyan@xmu.edu.cn; kelvinzhang@xmu.edu.cn

Metal oxides are promising (photo)electrocatalysts for sustainable energy technologies due to their good activity and abundant resources. Their applications such as photocatalytic water splitting predominantly involve aqueous interfaces at electrochemical conditions, but in situ probing oxide-water interfaces is proven to be extremely challenging. Here, we present an electrochemical scanning tunneling microscopy (EC-STM) study on the rutile TiO_2(110)-water interface, and by tuning surface redox chemistry with careful potential control we are able to obtain high quality images of interfacial structures with atomic details. It is interesting to find that the interfacial water exhibits an unexpected double-row pattern that has never been observed. This finding is confirmed by performing a large scale simulation of a stepped interface model enabled by machine learning accelerated molecular dynamics (MLMD) at ab initio accuracy. Furthermore, we show that this pattern is induced by the steps present on the surface, which can propagate across the terraces by interfacial hydrogen bonds. Our work demonstrates that by combining EC-STM and MLMD we can obtain new atomic details of interfacial structures that are valuable to understand the activity of oxides at realistic conditions.

Earth-abundant metal oxides are among the most promising (photo)electrocatalysts in a wide range of environmental and energy applications owing to their excellent activity, low costs and high stability at reactive conditions.[1–4] Since the vast majority of these reactions operate in solution, understanding oxide-water interfaces at atomic level is prerequisite for elucidating fundamental mechanisms and rationally optimising catalytic performances.[5] Thus, tremendous efforts, both experimentally and computationally, have been devoted to revealing the microscopic details of the interfaces. For example, X-ray absorption[6], Raman[7] and sum frequency generation spectroscopies[8,9] have been developed to in situ probe the interfaces, and can provide valuable interfacial information, often helped by density functional theory (DFT) calculation for interpreting spectra.[10,11]

Among those techniques, scanning tunneling microscopy (STM) has a prominent position and can directly offer images of atomic structures of the surfaces. Combination of STM and DFT has been the workhorse for development of oxide surface science in ultrahigh vacuum (UHV), most notably on the all-important model system TiO_2.[12–17] Somewhat in parallel, electrochemical STM (EC-STM) has been developed in the electrochemistry community for probing interfacial structures on metal electrodes.[18–22] However, it is very challenging to operate EC-STM on oxides, due to various difficulties such as low electrical conductivity, preparation of clean, atomically flat surfaces and potential control of imaging conditions. As a result, EC-STM studies on oxides are rare, and limited information can be extracted.[23–25]

Here, we present a combined EC-STM and machine learning accelerated molecular dynamics (MLMD) study on single crystal rutile TiO_2(110) surface at electrochemical conditions (Figure 1). Fine tuning the electrode potential condition of the oxide substrate enables us to play with the surface redox chemistry, leading to high quality STM images with atomic details of interfacial structures. We discover that the TiO_2(110) surface at electrochemical conditions exhibits an unexpected double-row pattern, which has not been observed at UHV and low vapor pressure conditions. We then utilize MLMD that affords long time scale simulations[26–28] of large interface models at ab initio accuracy (Figure 1(c)), to reveal that this special pattern can be assigned to the adsorbed water at five-coordinated Ti (Ti_{5c}) trough that shows a universal shift away from the centre to the row of bridge oxygen. What is surprising is that this asymmetric structure results from the biased water configurations at the [1$\bar{1}$1] steps present at the edges of terraces of width of hundreds of nanometers on single crystal TiO_2(110) surface. Our work demonstrates that distinct from that in vacuum, the interfacial water structure on TiO_2(110) is subjected to a long range effect due to the symmetry breaking boundary of step edges, which are expected to be widely applicable to nanostructures with finite facets at realistic environments.

Results

The rutile TiO_2 (110) surface was prepared by HF etching, followed by annealing at 950 °C in oxygen flow. This treatment[29] can give very high-quality, atomically flat surface with

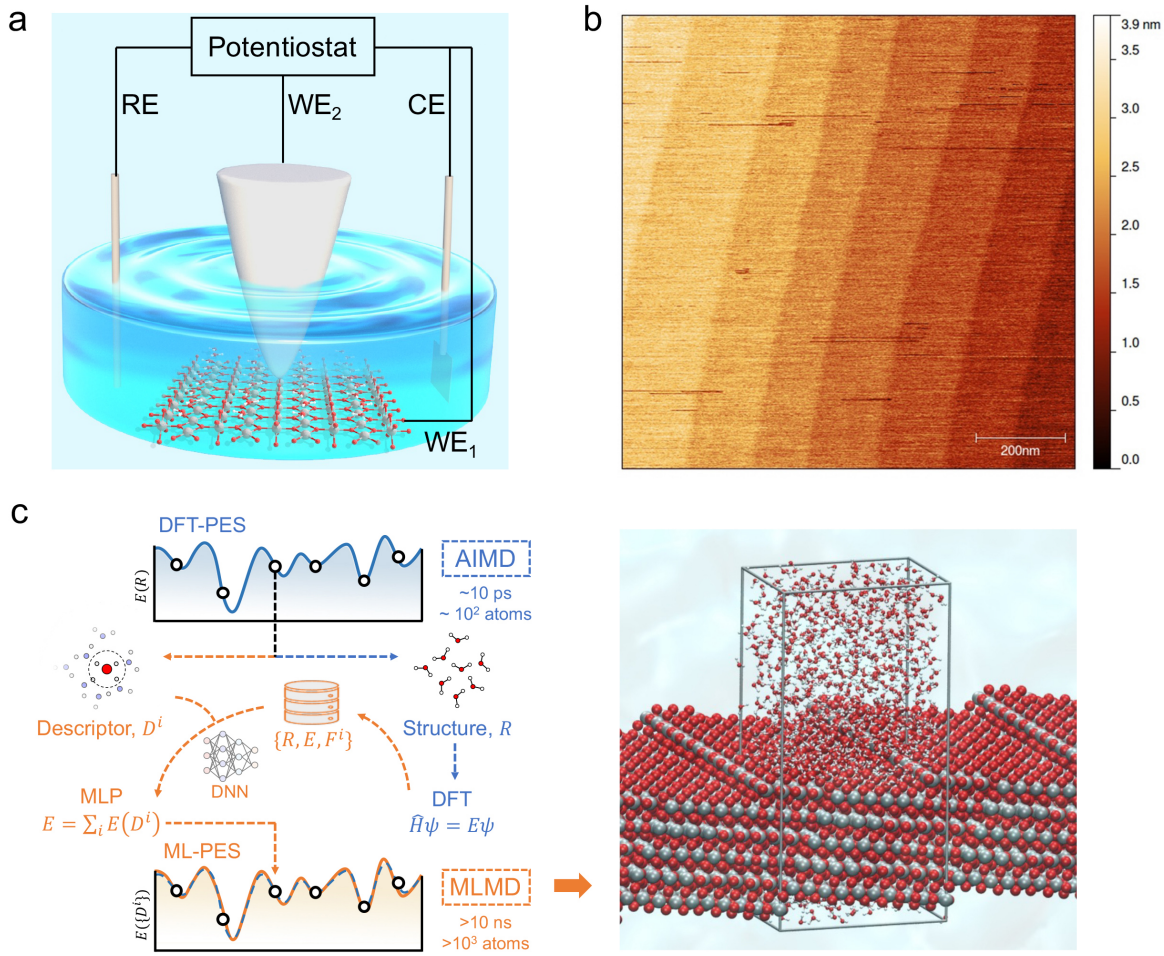

Figure 1. (a) Schematic illustration of EC-STM cell. The four-electrode setup consists of a working oxide substrate (WE_1), STM tip (WE_2), counter electrode (CE) and quasi-reference electrode (RE). (b) AFM image of rutile TiO_2 (110) surface with the size of $1 \times 1\ \mu m^2$. The measured step height is 3.2±0.5 Å. (c) Schematic illustration of MLMD simulation of the rutile TiO_2(110)-water interface with a $[1\bar{1}1]$ step, where Ti, O and H atoms are coloured in grey, red and white, respectively. The high computational costs of DFT calculation limit ab initio molecular dynamics (AIMD) to simulate models of $\sim 10^2$ atoms at a time scale of ∼10 ps. When trained with deep neural network (DNN) on a relative small set of data generated from DFT, energies and forces can be predicted by machine learning potentials (MLP) from structural descriptors at ab initio accuracy. The difference between machine learned potential energy surface (ML-PES) and DFT-PES is negligible. Due to the high efficiency, MLMD enables much longer simulations of larger models at lower costs.

terrace width of ∼200 nm and atomic step height of 3.2 ± 0.5 Å, as shown by the atomic force microscopy (AFM) image (see Figure 1(b) and also Figure S1 in the Supplementary Information (SI)). We first investigated the electrochemistry of the rutile TiO_2(110) in 0.1 M $HClO_4$ using cyclic voltammetry (CV). As shown in Figure 2(a), a pair of redox peaks at around -0.25 V vs Saturated Calomel Electrode (SCE) are clearly observed, which can be assigned to the surface redox process ($Ti^{IV}O_2 + e^- \leftrightarrow Ti^{III}O_2$).[30] Note that these peaks are detected at a faster scan rate of 1 V s^{-1} and disappear at a lower scan rate of 0.02 V s^{-1} because the peak current is proportional to the scan rate and becomes too small at a low scan rate to be distinguished.[31] The EC-STM measurements were carried out in a four-electrode cell setup consisting of a working oxide substrate (WE_1), STM tip (WE_2), counter electrode (CE) and quasi-reference electrode (RE). Unlike STM operation under UHV conditions, EC-STM images are obtained by controlling the potential of the oxide substrate and STM tip independently (see Figure 1(a)). Interestingly, we find that high resolution STM images of the TiO_2 surface can be obtained when the substrate potential is tuned to -0.38∼-0.18 V vs SCE and at the same time the tip potential is maintained at the range of 0.27∼1.32 V vs SCE, as illustrated in Figure 2(b)(c)(d).

Before interpreting the STM images, it would be informative to first answer two important questions; (i) why do the two

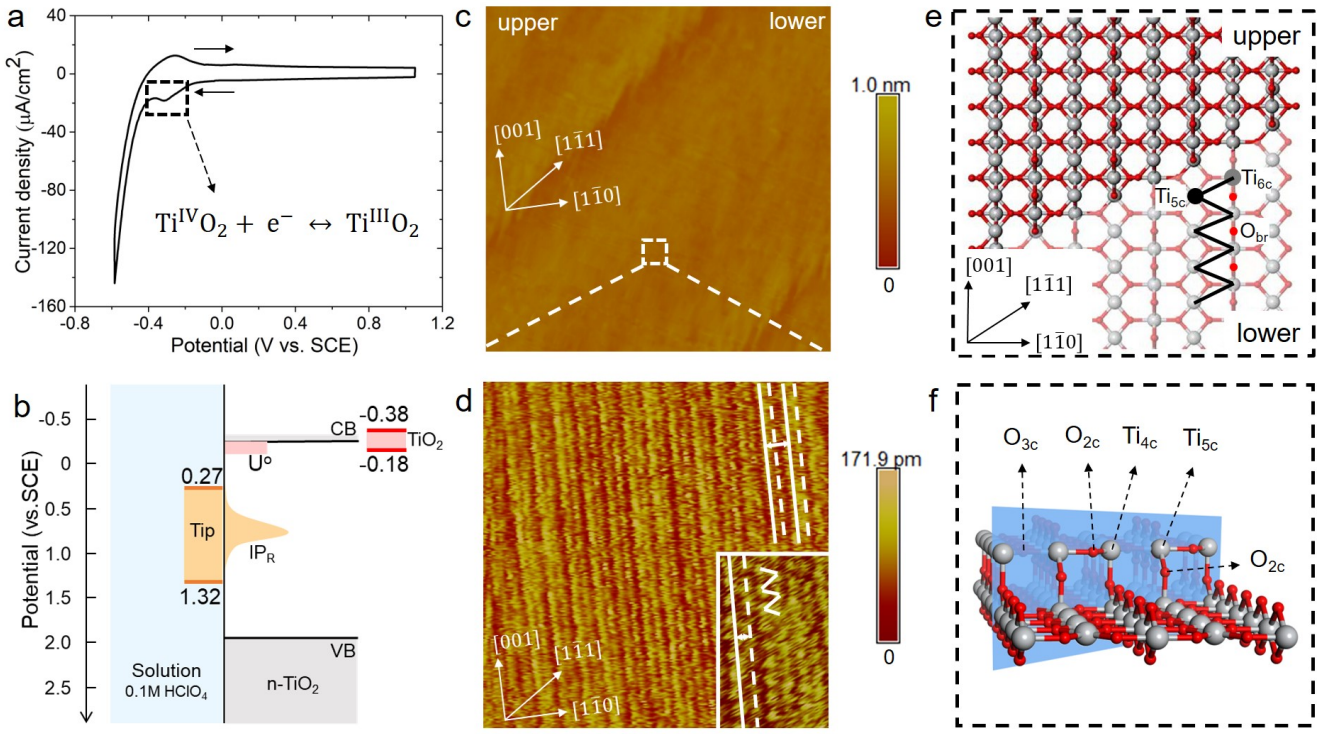

Figure 2. (a) Cyclic voltammogram of rutile TiO_2 (110) electrode in 0.1M $HClO_4$ at scan rate of 1 V s^{-1}. (b) Level diagram at the TiO_2 water interface in EC-STM configuration. The light red and orange region indicate the reduction potential of surface Ti^{IV}/Ti^{III} state (U°) and the vertical ionization potential of the corresponding reduced Ti^{III} state (IP_R), respectively. The red and orange range solid bars show the potential ranges of oxide sample and the STM tip adjusted to give high quality images. (c) Large area (150 × 150 nm^2) of EC-STM image of the rutile TiO_2 (110) in 0.1 M $HClO_4$. EC-STM parameters are E_{sample}=-0.38 V vs SCE, E_{tip}=1.27 V vs SCE, and I_{tunnel}=1 nA, respectively. (d) Magnified area (10 × 10 nm^2) with atomic resolution of the white dashed square in (c). The inset shows a further magnified area of 3 × 5 nm^2. (e) Top view of atomistic model of rutile TiO_2 (110) surface with a [1$\bar{1}$1] step. (f) Atomistic structure of the [1$\bar{1}$1] step. Ti and O atoms are coloured in grey and red, respectively.

potentials have to be tuned to these values? And (ii) why do they have to be set simultaneously? It is worth noting that the tuned substrate potential exactly overlaps with the reduction peak of CV in Figure 2(a), indicating that the TiO_2 surface just undergoes reduction to form surface Ti^{III}. On the other hand, it is well-known that on defective TiO_2 a band-gap state can be observed in X-ray photoelectron spectroscopy (XPS) around 0.9 eV below the conduction band minimum (CBM), which is associated with an excess electron occupying at the Ti 3d state.[32,33] By employing accurate hybrid density functional, Cheng and co-workers[34] calculated a number of reduced Ti^{III} states near the TiO_2 surface, and found that the redox levels of these states are near or just below the CBM while the corresponding vertical ionization potentials are about 0.6∼1.5 eV below the CBM. Putting all these levels together, we draw a level diagram as shown in Figure 2(b), and note that the band positions are adjusted to the pH = 1 condition according to the Nernstian relation. The two questions above can now be resolved as follows. Scanning the substrate potential to more negative than the reduction peak of the TiO_2 surface around -0.25 V vs SCE, the surface will be reduced to form band-gap states associated with Ti 3d states. These reduced, in-gap states, lying in about 1 eV range centered around 1 eV below the CBM (i.e. 0.3∼1.3 V vs SCE), can then resonate with the STM tip adjusted to the same potential so that high resolution STM images can be collected. It should be noted that if the substrate potential is too negative, i.e. < -0.38 V vs SCE, the hydrogen evolution current becomes too large to obtain stable STM images (see Figure S3).

Figure 2(d) shows a high resolution STM image of the aqueous rutile TiO_2(110), as taken and magnified from the white dashed square on the terrace in Figure 2(c). Considering the dynamic electrochemical environment at ambient temperature, the image quality is excellent and adequate for analyzing the interfacial structure. At the imaging conditions mentioned above, the STM image obtained corresponds to the occupied in-gap states, suggesting that the bright rows represent the density of the excess electrons at reduced surface Ti sites along the [001] direction. As shown by the magnified area in the inset of Figure 2(d), the zig-zag pattern from the underly-

ing terminal and bridge Ti sites in the adjacent rows (Figure 2(e)) is also visible. Similar STM images were observed on defective TiO_2 at UHV condition.[35–37] There is however a noticeable difference in the STM pattern between the two conditions; the bright rows are evenly spaced in UHV, while at electrochemical conditions a doubly alternating pattern of the bright rows can be clearly identified, which was not recoganizable in previous STM studies on aqueous TiO_2 surface.[24,25] It should be stressed that this double-row pattern has excellent reproducibility, and more high resolution STM images with same double-row spacing obtained by different tips from different experiments are illustrated in Figure S4. The good repeatability of the double-row spacing can effectively eliminate the possibility that the double-row pattern may be caused by the double tip[38], because the spacing of double row caused by double tip would change with the spacing of double tip in different experiments. It is also worth mentioning that this pattern is distinctly different from the double-strand structure of (1×2) on TiO_2(110) observed in UHV-STM, which has been ascribed to Ti_2O_3 added row[39,40]. The distance between two vicinal double-rows, i.e. two solid white lines in Figure 2(d), is calibrated to be 6.60 ± 0.30 Å, which is very close to the lattice constant, 6.50 Å, of rutile TiO_2 (110) surface along the $[1\bar{1}0]$ direction, and is much less than the spacing of double strands of Ti_2O_3 added row (about 13 Å)[39,40]. Intriguingly, the distance between two adjacent bright rows (i.e. solid and dashed white lines) within a repeating unit is only 3.08 Å, which is considerably shorter than half of the lattice constant of 3.25 Å.

It is unlikely that the alternating double-row pattern reflects the actual distortion of the underlying lattice of TiO_2, and thus we tentatively hypothesize that it results from the interfacial water interacting with the oxide surface. However, it is still puzzling why neither has a similar pattern been observed on rutile TiO_2(110) in vacuum or at low water vapor pressures by STM experiments,[41–43] nor by ab initio molecular dynamics (AIMD) calculation of the TiO_2 water interface.[44–46] To resolve this puzzle, we train a machine learning potential (MLP) with an iterative concurrent learning protocol[47] for describing the TiO_2 water interface at ab initio accuracy, and the training procedure and validation of the MLP can be found in the SI. The commonly used model of rutile TiO_2(110) was first simulated with MLMD, and owing to the efficiency of MLP, we can readily afford significantly longer time scale of tens of ns, in contrast to tens of ps for AIMD. The finding is however the same; we do not see systematically biased configurations of surface water adsorbed at the terminal Ti sites. As illustrated in Figure 3(b), the horizontal distance between the adsorbed water and the bridge O atoms on the left ($d^{(l)}$) and right ($d^{(r)}$) are indeed the same, i.e. $d^{(l)}$=$d^{(r)}$=3.25 Å, from the MLMD trajectory.

Considering a large single crystal surface often contains some steps separating narrow terraces (see Figure 1(b)), we speculate that the symmetry breaking steps might play a role in forming the asymmetric double-row pattern. We thus build a

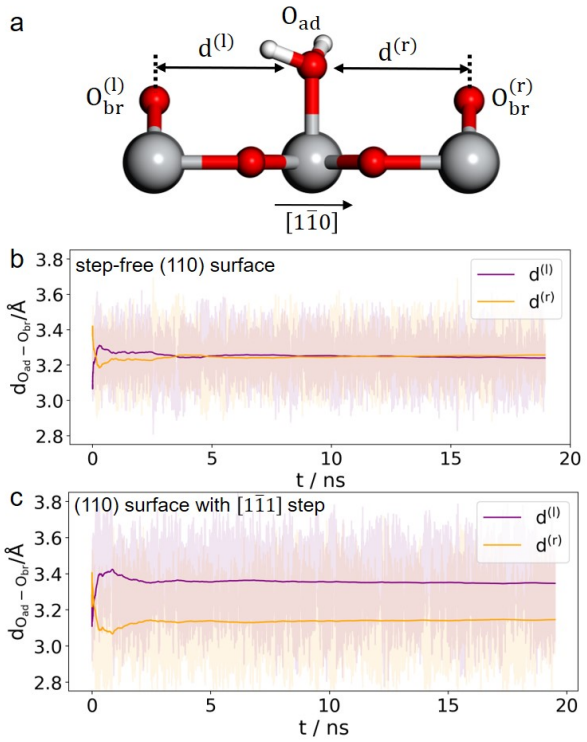

Figure 3. (a) Illustration of the horizontal distances between adsorbed water and the neighboring bridge O atoms. Time evolution of the O-O distances in step-free rutile TiO_2 (110) model (b) and that with a $[1\bar{1}1]$ step (c) from 20 ns MLMD trajectories. Ti, O and H atoms are coloured in grey, red and white, respectively.

large rutile TiO_2(110) surface model with an atomic $[1\bar{1}1]$ step separating terraces with 8 terminal Ti sites in a row (see Figure 1(c) and 2(e)(f)) according to previous studies[38,48]. Including water molecules, the interface model with a step consists of ~2000 atoms, about 10 times larger than the commonly used step-free model affordable to AIMD calculation. Somewhat unexpectedly, shortly after starting the MLMD run of the step model with unbiased configurations of surface water, all the adsorbed water molecules spontaneously shift away from the center to one side, and the horizontal distances to the left bridge oxygen and right become significantly different, $d^{(l)}$ = 3.35 Å and $d^{(r)}$ = 3.14 Å in Figure 3(c). To further validate the long range effect of the atomic step, we double the terrace width to about 5 nm with 16 terminal Ti sites, and this significantly larger model gives the same asymmetric structure of surface water (see more details in SI). To remove the effect of uncertainty in distance calibration in STM, we measure the ratio between the spacing of the two nearest rows in a double-row unit and the lattice of the repeating double-row pattern, to be 0.47, which is essentially the same as that from MLMD calculation. This quantitative agreement

is remarkable; not only does the MLMD calculation correctly represent the interfacial structure of the stepped surface, but also combination of experiment and theory strongly supports that the presence of the $[1\bar{1}1]$ steps on $TiO_2(110)$ causes the universal side shift of surface water.

The question then to be answered is why steps can shift adsorbed water on terraces. Carefully examining the water structure on the stepped surface from the MLMD trajectory, we notice that two terminal water molecules at the two ends of the Ti_{5c} trough may play a key role in shifting the whole row of surface water; one is located at the lower terrace of the step edge ("watA" in Figure 4(a)) and the other at the upper terrace ("watB" in Figure 4(b)). Near watA, there is a water adsorbed at the Ti_{4c} site of the step edge ("watC" in Figure 4(a)) forming strong hydrogen bonds (shorter distances than that in bulk water) with the step O_{2c} and the O_{br} at the lower terrace, as illustrated in Figure 4(a). The position of watC casts steric repulsion to watA, "pushing" it from the top site of octahedral coordination to the right along the $[1\bar{1}0]$ direction (Figure 4(c)). Also, watB can form a strong hydrogen bond with the bridge water at the step edge ("watD" in Figure 4(b)), thus being "pulled" to the right. Thus, the "push and pull" effect of the two edge terminal water triggers the side shift of the whole water row. Furthermore, this effect needs to be long-ranged as only a small fraction of steps are present on the surface. It can be proposed that the 1D hydrogen bond chain formed within the terminal water row and between the surface water and second water layer, propagates the shifting effect across the whole terraces, as illustrated in Figure 4(d). In addition, since this hydrogen bond chain is absent at UHV and low water vapor pressure conditions, it can be understood why the step-induced double-row pattern has not been observed in experiments carried out at these ideal conditions.

Discussion

To summarize, by combining EC-STM and MLMD, we show that the interfacial water on rutile $TiO_2(110)$ exhibits a doubly alternating pattern due to the presence of a small fraction of steps on the surface. This long range effect results from interfacial hydrogen bonds in aqueous environments, and is missing in previous studies in vacuum and at low water vapor pressures. Thus, our finding offers a new perspective to the interfacial structures, which may have important implications for understanding catalysis at realistic environments. We also show that by fine tuning the potential of the sample and STM tip, high resolution images of interfacial structures of oxides can be obtained at electrochemical conditions through surface redox chemistry. Therefore, our work opens up new opportunities for elucidating atomic structures of oxide-water interfaces with STM and MLMD, and we expect that such a surface redox mediated STM imaging mechanism could be developed for applications to interfaces at realistic conditions in a wider context.

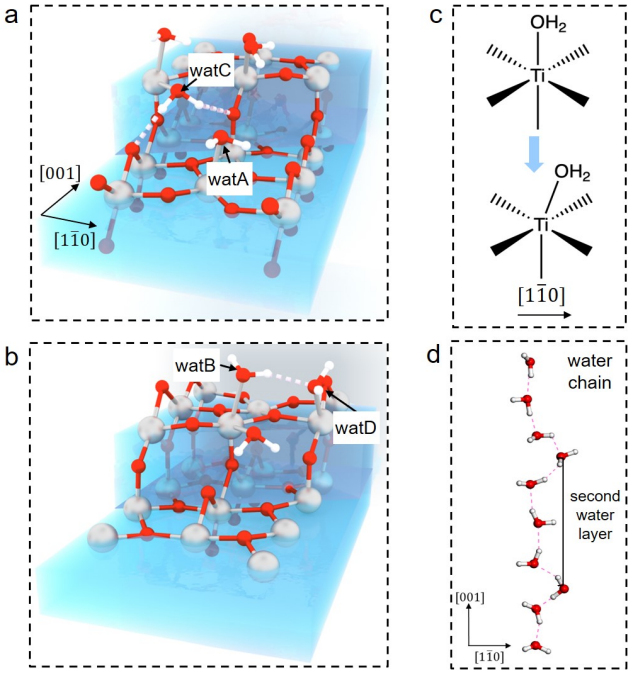

Figure 4. Schematic illustration of water structures at $[1\bar{1}1]$ step on rutile $TiO_2(110)$: (a) lower terrace (b) upper terrace. (c) Illustration of distortion of the octahedral coordination for adsorbed terminal water along $[1\bar{1}0]$ (d) Illustration of 1D hydrogen bond chain within the terminal water row and between surface water and second water layer on rutile TiO_2 (110). Ti, O and H atoms are coloured in grey, red and white, respectively.

Methods

Preparation of rutile TiO_2 (110) surface. The samples we used were 0.5 wt% Nb doped rutile TiO_2 (110) oriented single crystal (Crystec GmbH), which underwent chemical etching and annealing treatment to obtain atomically flat surfaces with $[1\bar{1}1]$ steps. The samples were treated by HF etching in buffered oxide etchant (BOE, NH_4F : HF = 10 : 1) and then annealed at 950 °C in the oxygen flow to obtain atomically smooth surfaces. Atomic force microscope (AFM) was performed by NanoWizard (JPK instruments).

Cyclic voltammetry. The electrochemical experiments were carried out on a single-chamber electrochemical cell. An AUTOLAB workstation (EcoChimie, Netherlands) equipped with fast scan SCAN250 module was used, and cyclic voltammetry was performed in linear mode optimized for fast process measurements. The electrolyte was 0.1 M perchloric acid solution prepared by perchloric acid (Merck, Suprapur) and ultra-pure water (18.2 MΩ · cm, Milli-Q), and the working electrode was rutile TiO_2 (110) single crystal. Prior to each experiment, the reference electrode silver wire and counter electrode platinum wire were boiled in ultra-pure water (18.2 MΩ · cm, Milli-Q) for at least three times for cleaning and stabilizing. After experiments, the reference electrode was immediately calibrated

to Saturated Calomel Electrode (SCE).

EC-STM setup. In-situ STM measurements were carried out on a Multimode VIII STM instrument (Bruker, Santa Barbara, CA) under constant current mode. The EC-STM tips, mechanically cut from a Pt/Ir wire (Pt80/Ir20; ϕ=0.25 mm), were insulated by thermosetting polyethylene to reduce Faradaic current, and they were stable in the potential window studied (see Figure S2 in SI). In the EC-STM cell, the working electrode was rutile TiO_2 (110) single crystal freshly prepared before each experiment, and the counter electrode was Pt wire. The electrolyte is 0.1 M $HClO_4$, prepared by perchloric acid (Merck, Suprapur) and ultra-pure water (18.2 M$\Omega \cdot$cm, Milli-Q). The reference electrode used was Pt quasi-reference electrode. The constant scan rate conducted in EC-STM was 30 Hz with 256 points per line for magnified images, corresponding to about 0.1 ms per image pixel, and for large area EC-STM images, the constant scan rate was 4 Hz.

Machine learning accelerated molecular dynamics. The machine learning potential adapted in this work is Deep Potential-Smooth Edition[49], and the training data were obtained by density functional theory calculation as implemented in the CP2K code.[50] The training data sets are generated with open-source deep potential generator package.[47] Details on training and validation of the machine learning potentials are given in the SI. The step-free rutile TiO_2 (110) surface was modelled by a symmetric periodic slab of five O-T-O tri-layers with a 8×4 supercell, and the size of the supercell is $23.67 \times 25.99 \times 38.53$ Å^3. For the surface with a $[1\bar{1}1]$ step, a 8×2 supercell was used with the exposure of the (9 10 1) surface, and the size is $27.02 \times 14.28 \times 48.15$ Å^3. The vacuum between the slabs is fully filled with water molecules, and as a result, the interface model of the step-free and stepped surface contain 2412 and 1785 atoms, respectively. The MLMD simulations were run by the LAMMPS package. NVT ensembles were imposed by the Nose-Hoover thermostat with the temperature of 330 K, and the MD time step was 0.5 fs.

References

1. Fujishima, A. & Honda, K. Electrochemical photolysis of water at a semiconductor electrode. *Nature* **238**, 37–38 (1972).
2. Chen, M. & Goodman, D. The structure of catalytically active gold on titania. *Science* **306**, 252–255 (2004).
3. Suntivich, J., May, K. J., Gasteiger, H. A., Goodenough, J. B. & Shao-Horn, Y. A perovskite oxide optimized for oxygen evolution catalysis from molecular orbital principles. *Science* **334**, 1383–1385 (2011).
4. Schneider, J. *et al.* Understanding TiO_2 photocatalysis: mechanisms and materials. *Chem. Rev.* **114**, 9919–9986 (2014).
5. Baker, L. R., Diebold, U., Park, J. Y. & Selloni, A. Oxide chemistry and catalysis. *J. Chem. Phys.* **153**, 050401 (2020).
6. Velasco Velez, J. J. *et al.* The structure of interfacial water on gold electrodes studied by X-ray absorption spectroscopy. *Science* **346**, 831–834 (2014).
7. Wang, Y. *et al.* In situ raman spectroscopy reveals the structure and dissociation of interfacial water. *Nature* **600**, 81–85 (2021).
8. McGuire, J. A. & Shen, Y. R. Ultrafast vibrational dynamics at water interfaces. *Science* **313**, 1945–1948 (2006).
9. Yang, D. *et al.* Facet-specific interaction between methanol and tio2 probed by sum-frequency vibrational spectroscopy. *Proc. Natl. Acad. Sci.* **115**, E3888–E3894 (2018).
10. Gaigeot, M.-P., Sprik, M. & Sulpizi, M. Oxide/water interfaces: how the surface chemistry modifies interfacial water properties. *J. Phys. Condens. Mat.* **24**, 124106 (2012).
11. Li, C. *et al.* In situ probing electrified interfacial water structures at atomically flat surfaces. *Nat. Mater.* **18**, 697–701 (2019).
12. Schaub, R. *et al.* Oxygen vacancies as active sites for water dissociation on rutile TiO_2 (110). *Phys. Rev. Lett.* **87**, 266104 (2001).
13. Diebold, U. The surface science of titanium dioxide. *Surf. Sci. Rep.* **48**, 53–229 (2003).
14. Bikondoa, O. *et al.* Direct visualization of defect-mediated dissociation of water on TiO_2 (110). *Nat. Mater.* **5**, 189–192 (2006).
15. Henderson, M. A. & Lyubinetsky, I. Molecular-level insights into photocatalysis from scanning probe microscopy studies on TiO_2 (110). *Chem. Rev.* **113**, 4428–4455 (2013).
16. Hussain, H. *et al.* Structure of a model TiO_2 photocatalytic interface. *Nat. Mater.* **16**, 461–466 (2017).
17. Balajka, J. *et al.* High-affinity adsorption leads to molecularly ordered interfaces on TiO_2 in air and solution. *Science* **361**, 786–789 (2018).
18. Tao, N. Probing potential-tuned resonant tunneling through redox molecules with scanning tunneling microscopy. *Phys. Rev. Lett.* **76**, 4066 (1996).
19. Fu, Y. *et al.* Supramolecular aggregation of inorganic molecules at au (111) electrodes under a strong ionic atmosphere. *J. Am. Chem. Soc.* **131**, 14728–14737 (2009).
20. Pfisterer, J. H., Liang, Y., Schneider, O. & Bandarenka, A. S. Direct instrumental identification of catalytically active surface sites. *Nature* **549**, 74–77 (2017).
21. Jacobse, L., Huang, Y., Koper, M. & Rost, M. J. Correlation of surface site formation to nanoisland growth in the electrochemical roughening of Pt (111). *Nat. Mater.* **17**, 277–282 (2018).

22. Wang, X. *et al.* In situ scanning tunneling microscopy of cobalt-phthalocyanine-catalyzed CO_2 reduction reaction. *Angew. Chem. Int. Ed.* **59**, 16098–16103 (2020).

23. Itaya, K. & Tomita, E. In-situ scanning tunneling microscopy of semiconductor (n-TiO_2)/liquid interfaces: a role of band bending in semiconductors. *Chem. Lett.* **18**, 285–288 (1989).

24. Serrano, G. *et al.* Molecular ordering at the interface between liquid water and rutile TiO_2 (110). *Adv. Mater. Interfaces* **2**, 1500246 (2015).

25. Müllner, M., Balajka, J., Schmid, M., Diebold, U. & Mertens, S. F. Self-limiting adsorption of WO_3 oligomers on oxide substrates in solution. *J. Phys. Chem. C* **121**, 19743–19750 (2017).

26. Behler, J. & Parrinello, M. Generalized neural-network representation of high-dimensional potential-energy surfaces. *Phys. Rev. Lett.* **98**, 146401 (2007).

27. Bartók, A. P., Payne, M. C., Kondor, R. & Csányi, G. Gaussian approximation potentials: The accuracy of quantum mechanics, without the electrons. *Phys. Rev. Lett.* **104**, 136403 (2010).

28. Zhang, L., Han, J., Wang, H., Car, R. & E, W. Deep potential molecular dynamics: a scalable model with the accuracy of quantum mechanics. *Phys. Rev. Lett.* **120**, 143001 (2018).

29. Yamamoto, Y., Nakajima, K., Ohsawa, T., Matsumoto, Y. & Koinuma, H. Preparation of atomically smooth TiO_2 single crystal surfaces and their photochemical property. *Jpn. J. Appl. Phys.* **44**, L511 (2005).

30. Wang, H. *et al.* Electrochemical investigation of traps in a nanostructured TiO_2 film. *J. Phys. Chem. B* **105**, 2529–2533 (2001).

31. Berger, T., Lana-Villarreal, T., Monllor-Satoca, D. & Gómez, R. An electrochemical study on the nature of trap states in nanocrystalline rutile thin films. *J. Phys. Chem. C* **111**, 9936–9942 (2007).

32. Henrich, V. E., Dresselhaus, G. & Zeiger, H. Observation of two-dimensional phases associated with defect states on the surface of TiO_2. *Phys. Rev. Lett.* **36**, 1335 (1976).

33. Wendt, S. *et al.* The role of interstitial sites in the Ti_{3d} defect state in the band gap of titania. *Science* **320**, 1755–1759 (2008).

34. Cheng, J., Liu, X., VandeVondele, J. & Sprik, M. Reductive hydrogenation of the aqueous rutile TiO_2 (110) surface. *Electrochim. Acta* **179**, 658–667 (2015).

35. Minato, T. *et al.* The electronic structure of oxygen atom vacancy and hydroxyl impurity defects on titanium dioxide (110) surface. *J. Chem. Phys.* **130**, 124502 (2009).

36. Yim, C. *et al.* Engineering polarons at a metal oxide surface. *Phys. Rev. Lett.* **117**, 116402 (2016).

37. Guo, C. *et al.* Probing nonequilibrium dynamics of photoexcited polarons on a metal-oxide surface with atomic precision. *Phys. Rev. Lett.* **124**, 206801 (2020).

38. Diebold, U. *et al.* Intrinsic defects on a TiO_2 (110)(1$\times$ 1) surface and their reaction with oxygen: a scanning tunneling microscopy study. *Surf. Sci.* **411**, 137–153 (1998).

39. Onishi, H., Fukui, K.-i. & Iwasawa, Y. Atomic-scale surface structures of TiO_2 (110) determined by scanning tunneling microscopy: a new surface-limited phase of titanium oxide. *Bull. Chem. Soc. Jpn.* **68**, 2447–2458 (1995).

40. Takakusagi, S., Fukui, K.-i., Nariyuki, F. & Iwasawa, Y. Stm study on structures of two kinds of wide strands formed on TiO_2 (110). *Surf. Sci.* **523**, L41–L46 (2003).

41. Pang, C. L., Lindsay, R. & Thornton, G. Structure of clean and adsorbate-covered single-crystal rutile TiO_2 surfaces. *Chem. Rev.* **113**, 3887–3948 (2013).

42. Wendt, S. *et al.* Oxygen vacancies on TiO_2 (110) and their interaction with H_2O and O_2: A combined high-resolution stm and dft study. *Surf. Sci.* **598**, 226–245 (2005).

43. Wang, Z.-T. *et al.* Probing equilibrium of molecular and deprotonated water on TiO_2 (110). *Proc. Natl. Acad. Sci.* **114**, 1801–1805 (2017).

44. Liu, L., Zhang, C., Thornton, G. & Michaelides, A. Structure and dynamics of liquid water on rutile TiO_2 (110). *Phys. Rev. B* **82**, 161415 (2010).

45. Cheng, J. & Sprik, M. Aligning electronic energy levels at the tio 2/h 2 o interface. *Phys. Rev. B* **82**, 081406 (2010).

46. Calegari Andrade, M. F., Ko, H., Car, R. & Selloni, A. Structure, polarization, and sum frequency generation spectrum of interfacial water on anatase TiO_2. *J. Phys. Chem. Lett.* **9**, 6716–6721 (2018).

47. Zhang, Y. *et al.* DP−GEN: A concurrent learning platform for the generation of reliable deep learning based potential energy models. *Comput. Phys. Commun.* **253**, 107206 (2020).

48. Zheng, T., Wu, C., Chen, M., Zhang, Y. & Cummings, P. T. A DFT study of water adsorption on rutile TiO_2 (110) surface: The effects of surface steps. *J. Chem. Phys.* **145**, 044702 (2016).

49. Wang, H., Zhang, L., Han, J. & E, W. DeePMD-kit: A deep learning package for many-body potential energy representation and molecular dynamics. *Comput. Phys. Commun.* **228**, 178–184 (2018).

50. VandeVondele, J. *et al.* Quickstep: fast and accurate density functional calculations using a mixed gaussian and plane waves approach. *Comput. Phys. Commun.* **167**, 103–128 (2005).

Acknowledgements

We acknowledge the funding support by National Natural Science Foundation of China (Grant Nos. 21991151, 21991150, 21861132015, 22021001, 92161113, 91945301, 22072123, 21872116 and 22225302) and Xiamen Science and Technology Plan Project (No. 3502Z20203027). We thank J.Wang, Y.J.Liu and T.Y.Ding for the help with illustration. Y. S. thanks J. Wang, Y.-J. Liu and T.-Y. Ding for the support on figure preparation.

Author contributions statement

J. C. conceived and designed the project. J. C., J.-W. Y. and K. H.-L. Z. supervised the experiment and calculation. Y. S. performed the EC-STM and AFM experiment, C.-R. W. prepared the single crystal samples, Y. S.and S. L. carried out the CV experiment. R.-H. B., Y.-B. Z. and F. W. performed the calculations. All the authors analysed the results and co-wrote the manuscript.

Competing interests

The authors declare no competing interests.

Additional information

Supplementary information is available online. Reprints and permissions information is available online. Correspondence should be addressed to J. C., J.-W. Y. and K. H.-L. Z.